

Effect of spin-orbit coupling on spectral and transport properties of tubular electron gas in InAs nanowires

I.A. Kokurin^{1,2,*}

¹*A. F. Ioffe Physical-Technical Institute, Russian Academy of Sciences, 194021 St. Petersburg, Russia*

²*Institute of Physics and Chemistry, Mordovia State University, 430005 Saransk, Russia*

(Dated: April 5, 2024)

We constructed the Hamiltonian of spin-orbit splitting for carriers of a tubular electron gas in InAs nanowires. The spectral problem is solved using an exact numerical diagonalization. It is shown that the contribution of k -linear Dresselhaus-like spin-orbit (SO) coupling leads to renormalization of so-called SO-gaps and appearance of anticrossings in subband spectrum. These features can be detected in ballistic transport.

I. INTRODUCTION

Nanowires (NWs) of narrow gap III-V semiconductors (such as InAs) attract significant interest in the field of modern nanoelectronics. NW is a good candidate for application in nanodevices such as field effect transistor (FET) [1, 2]. The near-surface band bending and Fermi-level pinning lead to formation of a two-dimensional electron gas (2DEG) close to the surface of an InAs NW [3]. Thus, a one-dimensional (1D) tubular conducting channel arises near the NW surface (see Fig. 1a). Furthermore, the asymmetric confinement of such an tubular electron gas (TEG) leads to strong spin-orbit coupling (SOC) of Rashba type [4]. A possibility of SOC strength tuning by gates of different geometry [5] allows to utilize the NWs in spintronics, e.g. as the basic element of Datta-Das spin-FET [6] or a gate-defined spin-orbit qubit [7].

Ballistic transport is preferable for spintronic nanodevices but implementation of the ballistic transport regime in InAs NWs has long hampered due to low carrier mobility that is determined by the surface roughness scattering. Nevertheless, it was recently shown that the ballistic transport can be realized in short InAs NWs [2].

The effect of Rashba SOC (RSOC) on the energy spectrum and ballistic transport in InAs NW was recently studied [8]. However, the influence of the lack of inversion center in semiconductor material constituting the nanostructure [9] was not considered. The so-called k -linear Dresselhaus SOC (DSOC) [9] arises from the following contribution to the Hamiltonian of Γ_6 conduction band of bulk III-V semiconductor [10]

$$H_D = \gamma \boldsymbol{\sigma} \boldsymbol{\kappa}, \quad (1)$$

where γ is the bulk Dresselhaus parameter and vector $\boldsymbol{\kappa} = (\kappa_x, \kappa_y, \kappa_z)$ has components $\kappa_x = k_x(k_y^2 - k_z^2)$ and κ_y, κ_z can be obtained by cyclic permutations, and $\boldsymbol{\sigma} = (\sigma_x, \sigma_y, \sigma_z)$ is the vector of Pauli matrices. It should

be noted that this operator is written in principle axes, i.e. $x||[100]$ etc. It is obvious that dimension lowering (to 2D or 1D) results in orientation-dependent SOC. NWs usually grows at orientation along $[111]$ -direction. The specificity of TEG is that electrons undergo different DSOC in each point of NW cross-section in contrast to usual planar structures [11, 12].

In present work we study the effect of SOC on spectral properties of NW using the simple model of 2DEG placed on a cylindrical surface [13]. The ballistic transport (conductance and thermopower) is studied as well.

II. HAMILTONIAN AND SPECTRAL PROBLEM

The $[111]$ -grown NWs as a rule have a hexagonal cut. However, the most authors do not take into account this fact and suppose the NW cross-section to be circular [3, 14, 15]. Here we use the simple model of 2DEG placed on cylindrical surface [13]. The possibility of this model application to TEG of radius r_0 (see Fig. 1a) in InAs NW was discussed in Ref. [8]. The Hamiltonian of the system can be written in the form $H = H_k + H_R + H_D$, where H_k is the kinetic term and $H_{R(D)}$ is the operator of RSOC (DSOC). If the magnetic field \mathbf{B} is included in consideration then the Zeemann splitting H_Z has to be taken into account and we have to include the influence of magnetic field on orbital motion by substitution $\mathbf{p} \rightarrow \mathbf{p} - (e/c)\mathbf{A}$ with \mathbf{p} and \mathbf{A} being the electron momentum and vector potential, respectively. In this case the Hamiltonian of the system with RSOC only $H_0 = H_k + H_R + H_Z$ is given by [8]

$$H_0 = \frac{\Pi_z^2 + \Pi_\varphi^2}{2m} + \frac{\alpha}{\hbar}(\sigma_z \Pi_\varphi - \sigma_\varphi \Pi_z) + \frac{1}{2}g^*\mu_B B \sigma_z, \quad (2)$$

where $m, g^*, \mu_B = |e|\hbar/2m_0c$ are the effective mass, g -factor and Bohr magneton, respectively, $\boldsymbol{\Pi} = \mathbf{p} - \frac{e}{c}\mathbf{A}$ is the kinematic momentum and $p_z = -i\hbar\partial/\partial z$, $p_\varphi = -(i\hbar/r_0)\partial/\partial\varphi$. We use the following gauge of vector potential, ($A_\varphi = Br_0/2, A_z = 0$). Here we use the ‘cylindrical’ Pauli matrices $\sigma_r(\varphi) = \cos\varphi\sigma_x + \sin\varphi\sigma_y$, $\sigma_\varphi(\varphi) = -\sin\varphi\sigma_x + \cos\varphi\sigma_y$. The explicit form of $\sigma_r(\varphi)$

*Electronic address: kokurinia@math.mrsu.ru

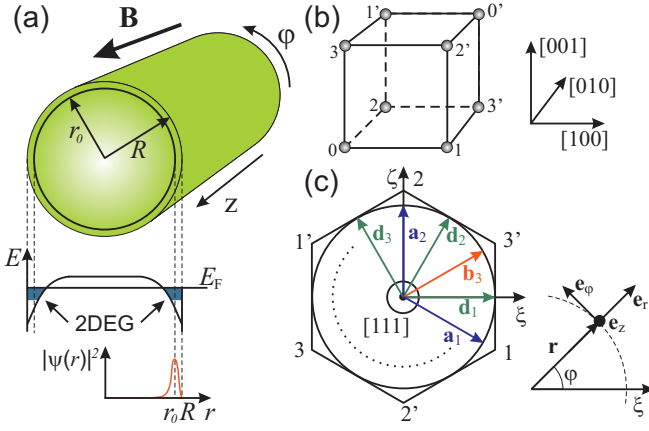


FIG. 1: (Color online) (a) Sketch of the InAs NW with radius R placed in longitudinal magnetic field \mathbf{B} . The band bending which leads to TEG formation is depicted. Carriers are concentrated in thin cylindrical layer of radius r_0 . The radial distribution is schematically shown. (b) The cubic cell of a zinc-blende lattice. Atoms of one sort (e.g. In) are shown in vertices of the cube. (c) The scheme that is needed for DSO Hamiltonian derivation. The sets of points 1, 2, 3 ($1'$, $2'$, $3'$) are projected on (111)-plane. The NW axis coincides with [111]-direction. Other vectors lie in (111)-plane. Any unit vector in this plane is determined by only one parameter (angle φ), see Appendix A. The polar frame of reference in plane (111) and unit vectors discussed in text are shown as well.

is

$$\sigma_r(\varphi) = \begin{pmatrix} 0 & e^{-i\varphi} \\ e^{i\varphi} & 0 \end{pmatrix}, \quad \sigma_\varphi(\varphi) = \begin{pmatrix} 0 & -ie^{-i\varphi} \\ ie^{i\varphi} & 0 \end{pmatrix}. \quad (3)$$

The spectrum of Hamiltonian (2) is given by

$$\frac{E_{jm}(k)}{E_0} = (kr_0)^2 + (j + \Phi/\Phi_0)^2 + 1/4 - \Lambda_R/2 + s\sqrt{(\Lambda_R kr_0)^2 + [\Delta - (1 - \Lambda_R)(j + \Phi/\Phi_0)]^2}, \quad (4)$$

where $E_0 = \hbar^2/2mr_0^2$ is the character energy scale in the problem, $\Lambda_R = 2m\alpha r_0/\hbar^2$ is the dimensionless RSOC parameter, and $j = \pm 1/2, \pm 3/2, \dots$ is z -projection of total angular momentum, $s = \pm 1$ numerates two branches of spin-splitted spectrum, Φ is the magnetic flux $\pi r_0^2 B$ through the section of TEG, $\Phi_0 = 2\pi\hbar c/|e|$ is the flux quantum, and $2\Delta = g^*\mu_B B/E_0$ is the dimensionless energy of Zeemann splitting.

Eigenstates of H_0 are given by

$$\Psi(\varphi, z) = \frac{e^{ikz}}{\sqrt{2\pi L}} \begin{pmatrix} e^{i(j-1/2)\varphi} C_{jk}^{(s)} \\ e^{i(j+1/2)\varphi} D_{jk}^{(s)} \end{pmatrix}, \quad (5)$$

where L is NW length, $\hbar k$ longitudinal momentum, and spinor components $C_{jk}^{(s)}$ and $D_{jk}^{(s)}$ are in general k -dependent due to SOC. Normalized eigenspinors are given

by

$$C_{jk}^{(+)} = D_{jk}^{(-)} = i \sin\left(\frac{\theta_{jk}}{2}\right), \quad D_{jk}^{(+)} = C_{jk}^{(-)} = \cos\left(\frac{\theta_{jk}}{2}\right), \quad (6)$$

with

$$\theta_{jk} = \arctan\left[\frac{\Lambda_R kr_0}{(1 - \Lambda_R)\lambda_j - \Delta}\right] + \pi\theta[\Delta - (1 - \Lambda_R)\lambda_j], \quad (7)$$

where $\theta(x)$ is the Heaviside unit step function and $\lambda_j = j + \Phi/\Phi_0$.

As was shown in Ref. [8] the strong SOC leads to appearance of so-called W-shape subbands (subbands with $s = -1$ can have 2 minima and 1 maximum). In this case the so-called SO-gaps first mentioned in Ref. [16] take place in the subband spectrum. This is the gap between maxima in W-shape subband and minima in higher lying subband (with single extremum) that is due to SOC.

Now we consider the effect of bulk inversion asymmetry (BIA) or so-called Dresselhaus effect [10] that take place in semiconductors without inversion center, such as InAs. In the used model of TEG for NW oriented along [111]-axis the k -linear Dresselhaus type spin-orbit Hamiltonian has the form

$$H_D = \frac{\beta}{\sqrt{6}} \left[-\frac{1}{\sqrt{2}} \left(\sigma_r(\varphi)k_\varphi - \frac{i}{2r_0}\sigma_\varphi(\varphi) \right) + \sigma_r(-2\varphi)k_z + 3\sigma_z \left(\sin 3\varphi k_\varphi - \frac{3i}{2r_0} \cos 3\varphi \right) \right], \quad (8)$$

where β is the k -linear DSO parameter (or BIA parameter), and $\hbar\mathbf{k} = \mathbf{p}$. Derivation of this operator is presented in Appendix A. The effect of magnetic field on operator H_D will be taken into account in standard manner. Using the above-mentioned gauge of vector potential it leads to the substitution $k_\varphi \rightarrow K_\varphi = k_\varphi + \frac{1}{r_0}\frac{\Phi}{\Phi_0}$.

One can see that operator H_D (8) and in turn the total Hamiltonian $H = H_0 + H_D$ do not commute with the operator of z -projection of total angular momentum $j_z = -i\hbar\frac{\partial}{\partial\varphi} + \frac{\hbar}{2}\sigma_z$ (the rotational invariance of the total Hamiltonian H is broken because DSO depends on crystallographic orientation), but H_D commutes with k_z (the translational invariance is conserved) that simplifies the following numerical diagonalization. This means that the states (5) which had definite j now will be mixed and anticrossings will appear in the energy spectrum.

Now we use 20×20 Hamiltonian (the matrix elements are calculated in basis of states (5) with $j = \pm 1/2, \dots, \pm 9/2$ and $s = \pm 1$) for numerical diagonalization that ensure a perfect precision for the spectrum of first 10 low-lying subbands. The result of numerical diagonalization is depicted in Fig. 2. The matrix elements of H_D , that we use, are written in Appendix B. The second and third terms of Eq. (8) mixes the states of subbands (j, s) and $(j \pm 3, \pm s)$. One can see in Fig. 2 the anticrossing that is due to mixing of states $(j = -3/2, s = +1)$ and $(j = 3/2, s = -1)$ by DSO Hamiltonian. Close to

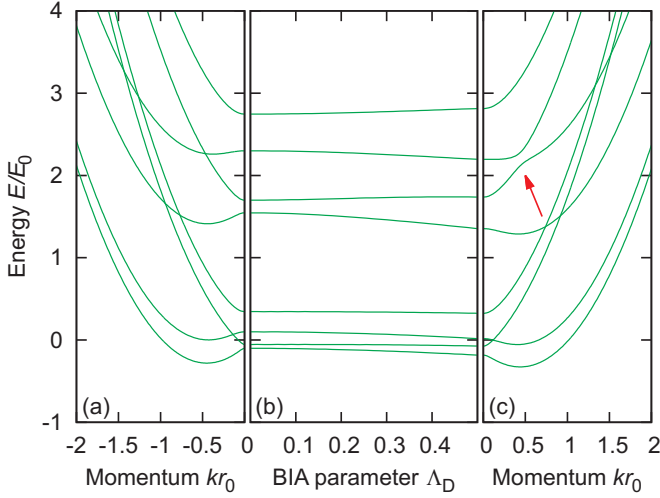


FIG. 2: (Color online) The effect of BIA SOC on the energy spectrum of InAs NW. (a) The subband energy spectrum. $\Lambda_R = 0.9$, $\Lambda_D = 0$, $\Phi = 0.15\Phi_0$. (b) The dependence of energy at $k = 0$ on dimensionless BIA parameter Λ_D . (c) The subband energy spectrum. $\Lambda_R = 0.9$, $\Lambda_D = 0.5$, $\Phi = 0.15\Phi_0$. An arrow indicates the anticrossing that is due to BIA SOC.

this anticrossing the energy spectrum can be described in more simple manner. In this case one can use the conventional perturbation theory for degenerate states and solve the secular equation for 2×2 Hamiltonian. However, the form of matrix elements (see Appendix B) does not allow to obtain a simple analytical result.

The DSOC Hamiltonian due to the first term in Eq.(8) increases so-called SO-gaps in spectrum that one can see in Fig. 2b. The first term in Hamiltonian (8) commutes with j_z -operator and has non-zero matrix elements (in basis (5)) only for $j = j'$ (see Appendix B). Thus, the spectral problem for reduced total Hamiltonian having only first term from H_D can be solved analytically (as in Ref. [8]). This leads to renormalization of SO-gaps width (in units of E_0)

$$\delta_j^{so} = 2\sqrt{[(1 - \Lambda_R)\lambda_j - \Delta]^2 + \Lambda_D^2 \lambda_j^2 / 12}, \quad (9)$$

that tends to Eq. (6) of Ref. [8] at $\Lambda_D = 2m\beta r_0/\hbar^2 \rightarrow 0$. However, taking into account the total H_D Hamiltonian, Eq. (9) is valid far from anticrossings (that are due to second and third term in Eq. (8)). When Λ_D increases up to 1 or more then the spectrum varies considerably. However, we suppose that in real InAs NW the condition $\alpha > \beta$ ($\Lambda_R > \Lambda_D$) fulfills by analogy with planar InAs nanostructures [17].

The energy distance between single maximum and two minima in W-shape subband is given by (using simplified Hamiltonian $H' = H_0 + H_{D1}$)

$$\delta_j^w = \frac{1}{\Lambda_R} \left(\frac{\Lambda_R^2}{2} - \sqrt{[(1 - \Lambda_R)\lambda_j - \Delta]^2 + \Lambda_D^2 \lambda_j^2 / 12} \right)^2. \quad (10)$$

Let us note that $(j, s = -1)$ -subband has W-shape form when the expression in brackets of Eq. (10) is positive. One can see from this equation the competition between RSOC and DSOC, i.e. the increasing of Λ_R leads to appearance of W-shape subbands, whereas the increasing of Λ_D suppress the emergence of such subbands. The increasing of δ_j^{so} and decreasing of δ_j^w is seen in Fig. 2 when BIA parameter Λ_D grows up. In next section we will see that the mentioned SO-gaps or their renormalization and disappearance of W-shape subbands can be detected in ballistic transport, namely in conductance and thermopower.

III. BALLISTIC TRANSPORT

If the 1D system have the complex spectrum (more than one extremum in any subband) then the ballistic conductance is given by [18]

$$G = \frac{G_0}{2} \sum_{in} \beta_i^n f(E_i^n, \mu, T). \quad (11)$$

Here $G_0 = e^2/\pi\hbar$ is the conductance quantum (for spin-degenerate case), $f(E, \mu, T)$ is the Fermi distribution function, μ and T are the chemical potential and temperature, respectively, E_i^n is the energy at n -th extremum of i -th subband, and $\beta_i^n = +1$ if n -th extremum of i -th subband is the minimum point but $\beta_i^n = -1$ if n -th extremum of i -th subband is the maximum one. The sum in (11) is over all extremal points of all subbands.

The dependence of NW conductance on the chemical potential at $T = 0$ is plotted in Fig. 3. One can see that conductance step-like behavior differs from one for 1D systems with simple parabolic dispersion when the conductance always increase with the chemical potential growing (see for instance Refs. [19, 20]). It is obvious that \sqcup -like plateaus are due to presence of consequent maxima and minima in the subband spectrum and the width of such a plateau is equal to corresponding SO-gap width δ_j^{so} . The comparison for the case of $\beta = 0$ and $\beta \neq 0$ is performed. One can see that at finite Λ_D there is a distortion of the picture at $\Lambda_D = 0$: the width of SO-gaps grows up at Λ_D increasing in accordance with Eq. (9). However, at high β ($\Lambda_D \sim 1$) the dependence $G(\mu)$ is significantly distorted. The temperature increasing leads to the smearing of conductance steps, since electrons coming in from reservoirs no longer have a sharp step-like energy distribution.

The contribution of W-shape subband, where 2 minima give $+G_0$ and a maximum gives $-G_0/2$ in accordance with Eq. (11), can be interpreted as a contribution of one electron and one hole subband. In this sense, if the chemical potential lies between minima and maximum then we have both electron and hole contribution $G_0/2 + G_0/2 = G_0$, and when the chemical potential lies higher than single maximum then we have only electron

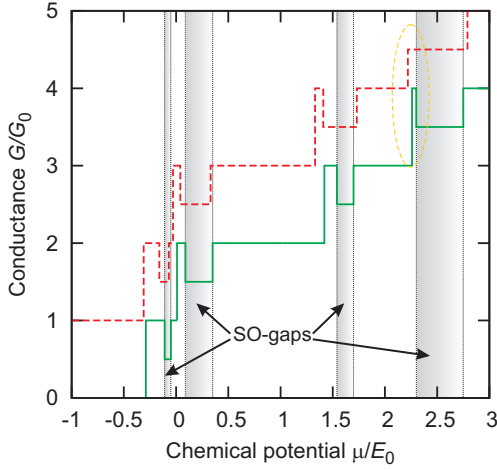


FIG. 3: (Color online) Conductance of InAs NW as a function of the chemical potential. $\Lambda_R = 0.9$, $\Phi = 0.15\Phi_0$, $T = 0$; full line, $\Lambda_D = 0$; dashed line, $\Lambda_D = 0.4$. Curves are vertically shifted for clarity. The areas corresponding to μ -values lying in SO-gaps are shaded.

contribution $+G_0/2$. Thus, the \sqcap -like plateau deals with a W-shape subband and its width is equal to δ_j^w (see Eq. (10)). In Fig. 3 close to $\mu = 2.2E_0$ one can see that finite Λ_D leads to disappearance of the W-like shape of one subband.

For the thermopower S we recently found the following expression [8]

$$S = \frac{k_B}{e} \frac{\sum_i \left[\ln 2 + \sum_n \beta_i^n F\left(\frac{E_i^n - \mu}{2T}\right) \right]}{\sum_{in} \beta_i^n f(E_i^n, \mu, T)}, \quad (12)$$

where the function $F(x) = \ln(\cosh x) - x \tanh x$ has the following properties: $F(-x) = F(x)$, $F(\pm\infty) = -\ln 2$, and $F(0) = 0$. The function $F[(E - \mu)/2T]$ as a function of the chemical potential μ represents a narrow symmetric peak with a width about several T .

The NW thermopower as a function of the chemical potential is plotted in Fig. 4. One can see the negative dips that is due to maxima in subband spectrum and it is unusual for systems with a simple parabolic dispersion [21–23]. By analogy with the conductance quantization these dips can be treated using the hole representation. It is worth noting that the peaks and dips take place at μ -values coinciding with energy extrema only approximately. The numerator in Eq. (12) has extrema at $\mu = E_i^n$, but in the vicinity of these points the denominator (dimensionless conductance) varies its own magnitude monotonically about 1 that leads to the shift of peak (dip) position and weak asymmetry of the peak (dip). Moreover, the mentioned deviation depends on the temperature: the position of peaks (dips) do not coincide with $\mu = E_i^n$ at high temperatures when the peaks (dips) overlap each other. Thus, the distance between consequent dip and peak approximately coincides with corresponding SO-gap (see Fig. 4). It is worth noted

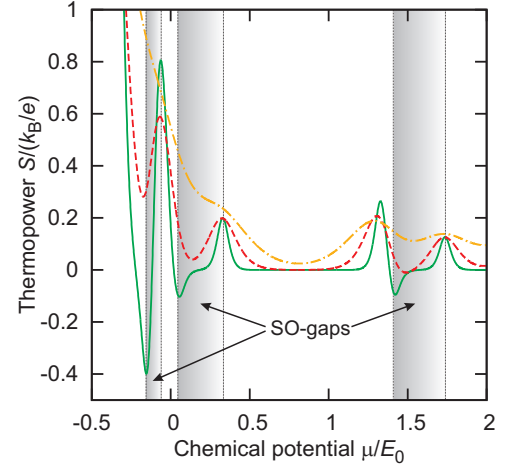


FIG. 4: (Color online) Thermopower of InAs NW as a function of the chemical potential. $\Lambda_R = 0.9$, $\Lambda_D = 0.4$, $\Phi = 0.15\Phi_0$; full line, $T = 0.02E_0$; dashed line, $T = 0.05E_0$; dot-dashed line, $T = 0.1E_0$. The areas corresponding to μ -values lying in SO-gaps are shaded.

that the temperature increasing leads to a disappearance of dips because of the widening of neighboring peaks of higher amplitudes.

At low temperatures (T is much less than energy distance between neighboring extrema) Eq.(12) is well approximated by so-called Mott formula [24] that connects the thermopower with conductance.

IV. CONCLUSION

Additionally to RSOC we constructed the DSOC Hamiltonian for TEG in [111]-oriented InAs NW and numerically solved the spectral problem. It is shown that DSOC lead to appearance of any specific features in the 1D subband spectrum, such as anticrossings, that was absent at RSOC consideration only. The effect of longitudinal magnetic field is also studied. The competition between two types of SOC was discussed. The ballistic conductance and thermopower of InAs NW were studied as well. At strong SOC the conductance step-like behavior differs from one for 1D systems with a simple parabolic dispersion, that is due to the presence of maxima in subband spectrum that in turn deals with strong SOC: the conductance can decrease with the Fermi energy increasing. Such an behavior of $G(\mu)$ -dependence looks like one that take place in semimetallic NW, when subbands of valence band and conduction one overlap one another, i.e. two types of charge carrier (electrons and holes) participate in the conduction process. The thermopower features are the negative dips in $S(\mu)$ dependence, i.e. S can change the sign with the chemical potential increasing. The reason of these features emergence is the same as for conductance decreasing and is due to strong SOC.

Acknowledgement

The author is grateful to N.S. Averkiev, A.M. Monakhov and L.E. Golub for useful discussions. This work has been supported by Russian Ministry of Education and Science (project No. 2665).

Appendix A: Derivation of k -linear Dresselhaus Hamiltonian on cylindrical surface

The hexagonal cut of [111]-grown NWs appears due to presence of C_3 symmetry axis. If we consider the cell of III-V semiconductor (a cube in Fig. 1b) then the projections of vertices of this cube onto (111)-plane form a hexagon. The coordinate of vectors from hexagon center to these vertices (see Fig. 1c) and to the middle of hexagon edges can be easily found from geometric consideration. Introducing the auxiliary planar frame of reference $\xi O\zeta$ (lying in (111)-plane), and choosing for the definiteness $\mathbf{e}_\xi = \mathbf{d}_1 = \frac{1}{\sqrt{2}}(0, -1, 1)$ and $\mathbf{e}_\zeta = \mathbf{a}_2 = \frac{1}{\sqrt{6}}(2, -1, -1)$ we find that the coordinates of any unit vector lying in (111)-plane will be determined by one parameter (azimuthal angle φ). We use here simple model supposing the NW cross-section to be circular and neglecting the hexagonal cut.

The cylindrical unit vectors have coordinates $\mathbf{e}_r = \cos\varphi\mathbf{e}_\xi + \sin\varphi\mathbf{e}_\zeta$, $\mathbf{e}_\varphi = -\sin\varphi\mathbf{e}_\xi + \cos\varphi\mathbf{e}_\zeta$, $\mathbf{e}_z = \frac{1}{\sqrt{3}}(1, 1, 1)$. Finally, we find for the vectors \mathbf{e}_r and \mathbf{e}_φ

$$\mathbf{e}_r = \sqrt{\frac{2}{3}} \left(\sin\varphi, -\cos\left(\varphi - \frac{\pi}{6}\right), \cos\left(\varphi + \frac{\pi}{6}\right) \right), \quad (\text{A1})$$

$$\mathbf{e}_\varphi = \sqrt{\frac{2}{3}} \left(\cos\varphi, \sin\left(\varphi - \frac{\pi}{6}\right), -\sin\left(\varphi + \frac{\pi}{6}\right) \right). \quad (\text{A2})$$

The straightforward procedure of derivation of k -linear DSOC Hamiltonian from Hamiltonian (1) in curvilinear coordinates is quite difficult problem. We propose here more simple approach: to construct the Hamiltonian for planar structure after that to apply it to non-planar surface taking into account not too large curvature.

Now we derive the k -linear DSOC Hamiltonian for planar two-dimensional (2D) structure grown along the axis lying arbitrary in plane (111). Consider planar 2D-structure that grown along vector $\mathbf{e}_{x'} \equiv \mathbf{e}_r$. Axis z' coincides with (111)-direction and y' is directed along \mathbf{e}_φ .

The coordinate transformation between crystallic coordinate system (xyz) and $x'y'z'$ reference frame performs by the following matrix

$$A = \frac{1}{\sqrt{3}} \begin{pmatrix} \sqrt{2}\sin\varphi & \sqrt{2}\cos\varphi & 1 \\ -\sqrt{2}\cos\left(\varphi - \frac{\pi}{6}\right) & \sqrt{2}\sin\left(\varphi - \frac{\pi}{6}\right) & 1 \\ \sqrt{2}\cos\left(\varphi + \frac{\pi}{6}\right) & -\sqrt{2}\sin\left(\varphi + \frac{\pi}{6}\right) & 1 \end{pmatrix}. \quad (\text{A3})$$

Usually at any rotation the spin matrix have to be transformed by means on finite rotations matrices. However, for the case of spin 1/2 this transformation is simplified and the Pauli matrices transform as components of usual vector [25]. Applying the last transformation to spin matrices σ_i and to components of wavevector k_j of (1) after tedious algebra and quantization of transformed k^3 -Hamiltonian to 2D one [9] we find (here we omit primes in coordinate subscripts)

$$H_D = \frac{\beta}{\sqrt{6}} \left(-\frac{1}{\sqrt{2}}\sigma_x k_y + \cos 3\varphi \sigma_x k_z - \sin 3\varphi \sigma_y k_z + 3 \sin 3\varphi \sigma_z k_y \right), \quad (\text{A4})$$

where $\beta = \gamma \langle k_x^2 \rangle \simeq \gamma (\pi/w)^2$ with w being the width of 2D layer and $\langle \dots \rangle$ denotes the averaging on the ground state of transverse motion. Here we take into account that $\langle k_x \rangle = \langle k_x^3 \rangle = 0$ and neglect the remaining k^3 -terms owing to inequality $\langle k_x^2 \rangle \gg k_{y(z)}^2$.

It should be noted, that the symmetry analysis lead to the Hamiltonian having all 6 possible terms (3 spin matrices multiplied by 2 components of wavevector) for the group C_1 (having the trivial symmetry operation only), but an exact calculation gives only 4 contributions. However, there is no contradiction, because 2 other terms can arise from high-power contribution in bulk spin-splitting Hamiltonian, e.g. from k^5 -splitting. Moreover, the form of the Hamiltonian (A4) depends on the origin of angle φ . Such a form take place when we suppose $\varphi = 0$ to be corresponding to orientation along $[0\bar{1}1]$ -direction.

Assuming the TEG radius r_0 to be much larger than the lattice parameter we obtain the Hamiltonian on the cylindrical surface from planar one (A4) by means of the following substitution

$$k_y \rightarrow k_\varphi, \quad \sigma_y \rightarrow \sigma_\varphi(\varphi), \quad \sigma_x \rightarrow \sigma_r(\varphi). \quad (\text{A5})$$

Since in cylindrical coordinates some of Pauli matrices do not commute with the operator k_φ therefore we have to additionally symmetrize (i.e. $AB \rightarrow \{A, B\} = (AB + BA)/2$) obtained Hamiltonian in order to ensure the Hermitianity. After that we obtain

$$H_D = \frac{\beta}{\sqrt{6}} \left[-\frac{1}{\sqrt{2}} \{ \sigma_r(\varphi), k_\varphi \} + \cos 3\varphi \sigma_r(\varphi) k_z - \sin 3\varphi \sigma_\varphi(\varphi) k_z + 3 \sigma_z \{ \sin 3\varphi, k_\varphi \} \right]. \quad (\text{A6})$$

If we take into account the explicit action of operators in symmetrized product then we obtain the final form of Hamiltonian (8).

Appendix B: Matrix elements of Dresselhaus Hamiltonian

For the sake of simplicity now we decompose the Hamiltonian (8) into 3 terms, $H_D = H_{D1} + H_{D2} + H_{D3}$, where

$$H_{D1} = -\frac{\beta}{\sqrt{12}} \left(\sigma_r(\varphi) K_\varphi - \frac{i}{2r_0} \sigma_\varphi(\varphi) \right), \quad (B1)$$

$$H_{D2} = \frac{\beta}{\sqrt{6}} \sigma_r(-2\varphi) k_z, \quad (B2)$$

$$H_{D3} = \sqrt{\frac{3}{2}} \beta \sigma_z \left(\sin 3\varphi K_\varphi - \frac{3i}{2r_0} \cos 3\varphi \right). \quad (B3)$$

The matrix elements of these operators calculated on eigenfunctions of Hamiltonian H_0 (5) are given by

$$\langle j' s' k' | H_{D1} | j s k \rangle = -\frac{\beta}{\sqrt{12} r_0} \delta_{kk'} \delta_{jj'} \lambda_j$$

$$\times \left(C_{jk}^{(s')*} D_{jk}^{(s)} + D_{jk}^{(s')*} C_{jk}^{(s)} \right), \quad (B4)$$

$$\begin{aligned} \langle j' s' k' | H_{D2} | j s k \rangle &= \frac{\beta}{\sqrt{6}} k \delta_{kk'} \\ &\times \left(\delta_{j,j'-3} C_{j'k}^{(s')*} D_{jk}^{(s)} + \delta_{j,j'+3} D_{j'k}^{(s')*} C_{jk}^{(s)} \right), \end{aligned} \quad (B5)$$

$$\begin{aligned} \langle j' s' k' | H_{D3} | j s k \rangle &= \sqrt{\frac{3}{2}} \beta \frac{\delta_{kk'}}{2ir_0} \\ &\times \left\{ \delta_{j,j'-3} \left[(\lambda_j + 1) C_{j'k}^{(s')*} C_{jk}^{(s)} - (\lambda_j + 2) D_{j'k}^{(s')*} D_{jk}^{(s)} \right] \right. \\ &\left. - \delta_{j,j'+3} \left[(\lambda_j - 2) C_{j'k}^{(s')*} C_{jk}^{(s)} - (\lambda_j - 1) D_{j'k}^{(s')*} D_{jk}^{(s)} \right] \right\} \end{aligned} \quad (B6)$$

The concrete form of any matrix elements can be found using the exact form of spinor components $C_{jk}^{(s)}$, $D_{jk}^{(s)}$ (see Eq.(6)).

-
- [1] S. A. Dayeh, D. P. R. Aplin, X. Zhou, P. K. L. Yu, E. T. Yu, D. Wang, High electron mobility inas nanowire field-effect transistors, *Small* 3 (2007) 326–332. doi:10.1002/sml.200600379.
- [2] S. Chuang, Q. Gao, R. Kapadia, A. C. Ford, J. Guo, A. Javey, Ballistic inas nanowire transistors, *Nano Lett.* 13 (2013) 555–558. doi:10.1021/nl3040674.
- [3] S. Estévez Hernández, M. Akabori, K. Sladek, C. Volk, S. Alagha, H. Hardtdegen, M. G. Pala, N. Demarina, D. Grützmacher, T. Schäpers, Spin-orbit coupling and phase coherence in inas nanowires, *Phys. Rev. B* 82 (2010) 235303. doi:10.1103/PhysRevB.82.235303.
- [4] Y. A. Bychkov, E. I. Rashba, Properties of a 2d electron gas with lifted spectral degeneracy, *JETP Lett.* 39 (1984) 78–81.
- [5] D. Liang, X. P. Gao, Strong tuning of rashba spinorbit interaction in single inas nanowires, *Nano Lett.* 12 (2012) 3263–3267. doi:10.1021/nl301325h.
- [6] S. Datta, B. Das, Electronic analog of the electro-optic modulator, *Appl. Phys. Lett.* 56 (1990) 665–667. doi:10.1063/1.102730.
- [7] S. Nadj-Perge, S. M. Frolov, E. P. A. M. Bakkers, L. P. Kouwenhoven, Spinorbit qubit in a semiconductor nanowire, *Nature* 468 (2010) 1084–1087. doi:10.1038/nature09682.
- [8] I. A. Kokurin, Determination of rashba-coupling strength for surface two-dimensional electron gas in inas nanowires, *Solid State Commun.* 195 (2014) 49 – 54. doi:10.1016/j.ssc.2014.07.002.
- [9] M. I. Dyakonov, V. Y. Kachorovskii, Spin relaxation of two-dimensional electrons in noncentrosymmetric semiconductors, *Sov. Phys. Semicond.* 20 (1986) 110.
- [10] G. Dresselhaus, Spin-orbit coupling effects in zinc blende structures, *Phys. Rev.* 100 (1955) 580–586. doi:10.1103/PhysRev.100.580.
- [11] S. Zhang, R. Liang, E. Zhang, L. Zhang, Y. Liu, Magnetosubbands of semiconductor quantum wires with rashba and dresselhaus spin-orbit coupling, *Phys. Rev. B* 73 (2006) 155316. doi:10.1103/PhysRevB.73.155316.
- [12] M. Wang, K. Chang, L. G. Wang, N. Dai, F. M. Peeters, Crystallographic plane tuning of charge and spin transport in semiconductor quantum wires, *Nanotechnology* 20 (2009) 365202. doi:10.1088/0957-4484/20/36/365202.
- [13] L. I. Magarill, D. A. Romanov, A. V. Chaplik, Kinetics of two-dimensional electrons on a curved surface, *JETP Lett.* 64 (1996) 460–466. doi:10.1134/1.567220.
- [14] S. Jin, J. Waugh, T. Matsuura, S. Faniel, H. Wu, T. Koga, Spin dependent electronic structure and level crossings as a function of magnetic field in inas nanowire, *Phys. Procedia* 3 (2010) 1321 – 1324. doi:http://dx.doi.org/10.1016/j.phpro.2010.01.184.
- [15] A. Bringer, T. Schäpers, Spin precession and modulation in ballistic cylindrical nanowires due to the rashba effect, *Phys. Rev. B* 83 (2011) 115305. doi:10.1103/PhysRevB.83.115305.
- [16] C. H. L. Quay, T. L. Hughes, J. A. Sulpizio, L. N. Pfeiffer, K. W. Baldwin, K. W. West, D. Goldhaber-Gordon, R. de Picciotto, Observation of a one-dimensional spin-orbit gap in a quantum wire, *Nature Phys.* 6 (2010) 336–339. doi:10.1038/nphys1626.
- [17] Y. Ho Park, H.-j. Kim, J. Chang, S. Hee Han, J. Eom, H.-J. Choi, H. Cheol Koo, Separation of rashba and dresselhaus spin-orbit interactions using crystal direction dependent transport measurements, *Appl. Phys. Lett.* 103 (2013) 252407. doi:10.1063/1.4855495.

- [18] Y. V. Pershin, J. A. Nesteroff, V. Privman, Effect of spin-orbit interaction and in-plane magnetic field on the conductance of a quasi-one-dimensional system, *Phys. Rev. B* 69 (2004) 121306. doi:10.1103/PhysRevB.69.121306.
- [19] M. Büttiker, Quantized transmission of a saddle-point constriction, *Phys. Rev. B* 41 (1990) 7906–7909. doi:10.1103/PhysRevB.41.7906.
- [20] E. N. Bogachek, M. Jonson, R. I. Shekhter, T. Swahn, Magnetic-flux-induced conductance steps in microwires, *Phys. Rev. B* 47 (1993) 16635–16638. doi:10.1103/PhysRevB.47.16635.
- [21] P. Streda, Quantised thermopower of a channel in the ballistic regime, *J. Phys.: Condens. Matter* 1 (1989) 1025–1027. doi:10.1088/0953-8984/1/5/021.
- [22] C. R. Proetto, Thermopower oscillations of a quantum-point contact, *Phys. Rev. B* 44 (1991) 9096–9099. doi:10.1103/PhysRevB.44.9096.
- [23] I. A. Kokurin, V. A. Margulis, A. V. Shorokhov, Thermopower of three-dimensional quantum wires and constrictions, *J. Phys.: Condens. Matter* 16 (2004) 8015. doi:10.1088/0953-8984/16/45/023.
- [24] M. Cutler, N. F. Mott, Observation of anderson localization in an electron gas, *Phys. Rev.* 181 (1969) 1336–1340. doi:10.1103/PhysRev.181.1336.
- [25] D. A. Varshalovich, A. N. Moskalev, V. K. Khersonskii, *Quantum Theory of Angular Momentum*, World Scientific, Singapore, 1988.